Peak electron densities in Saturn's ionosphere derived from the low-frequency cutoff of Saturn lightning

G. Fischer,[1,2] D. A. Gurnett,[2] P. Zarka,[3] L. Moore,[4] and U. A. Dyudina[5]

Received 6 October 2010; revised 24 January 2011; accepted 26 January 2011; published 21 April 2011.

[1] Radio bursts from Saturn lightning have been observed by the Cassini Radio and Plasma Wave Science instrument at frequencies of a few megahertz during several month-long storms since 2004. As the radio waves traverse Saturn's ionosphere on their way to the spacecraft, one can determine the peak electron density from the measurement of the low-frequency cutoff below which the radio bursts are not detected. In this way we obtained 231 profiles of peak electron densities that cover all Saturnian local times at a kronocentric latitude of 35°S, where the storms were spotted by the Cassini camera. Peak electron densities show a large variation at dawn and dusk and are around 5×10^4 cm^{-3}, in fair agreement with radio occultation measurements at midlatitudes. At noon and midnight, the densities are typically somewhat above 10^5 cm^{-3} and around 10^4 cm^{-3}, respectively. The diurnal variation is about 1 to 2 orders of magnitude for averaged profiles over one storm at 35°S. This is somewhat less compared to previous Voyager measurements which showed more than 2 orders of magnitude variation. The diurnal variation as well as the peak electron densities of Saturn's ionosphere tend to decrease with the decreasing solar EUV flux from 2004 until the end of 2009.

Citation: Fischer, G., D. A. Gurnett, P. Zarka, L. Moore, and U. A. Dyudina (2011), Peak electron densities in Saturn's ionosphere derived from the low-frequency cutoff of Saturn lightning, *J. Geophys. Res.*, *116*, A04315, doi:10.1029/2010JA016187.

1. Introduction

[2] The radio signatures of lightning from Saturn's atmosphere were first detected by the planetary radio astronomy (PRA) instrument on board Voyager 1, and *Warwick et al.* [1981] termed these impulsive radio bursts Saturn electrostatic discharges (SEDs). Initially there were some doubts about their atmospheric origin, and *Evans et al.* [1982] suggested that the SED source was located in Saturn's B ring. However, *Burns et al.* [1983] favored an atmospheric source and *Kaiser et al.* [1983] showed with an argument of visibility that the SEDs most likely originated from atmospheric lightning. The recurrence period of 10 h 09 min of the Voyager 1 SED episodes indicated an equatorial storm [*Zarka and Pedersen*, 1983].

[3] Typically, SEDs can be detected for about half a Saturn rotation when the storm is on the side facing the spacecraft and are absent when the storm is on the other side of the planet. This episodic occurrence of SEDs allows us to derive the approximate location of the lightning storm. The detection of SEDs should start/stop when the storm appears/disappears at the horizon as seen from the spacecraft. The Voyager 1 SED episodes lasted somewhat longer than half a Saturn rotation from which *Kaiser et al.* [1983] derived a longitudinal extension of the equatorial storm of 60°. The low-frequency cutoff of the SED episodes was then used by *Kaiser et al.* [1984] to compute the ionospheric peak electron density as a function of the storm's mean local time. They derived peak electron densities somewhat less than 10^3 cm^{-3} at midnight and somewhat greater than 10^5 cm^{-3} at noon, i.e., a diurnal variation of more than 2 orders of magnitude. For dawn and dusk the inferred density was ~10^4 cm^{-3} in agreement with the Voyager radio occultation data of *Lindal et al.* [1985]. Similarly, *Zarka* [1985a] also found this large diurnal variation and obtained somewhat higher values for the dayside equatorial ionosphere, but still within the error bars of *Kaiser et al.* [1984].

[4] So far, models of Saturn's ionosphere cannot reproduce the 2 order of magnitude diurnal variation inferred from the SEDs [*Nagy et al.*, 2009]. The first time-dependent ionospheric model of *Majeed and McConnell* [1996] showed much less variation due to the long chemical lifetime of the dominant H^+ ion relative to a 10–11 h Saturn day. Modern models, such as *Moses and Bass* [2000] and *Moore et al.* [2004] predicted that H^+ would be the dominant ion in the topside ionosphere and at night, but H_3^+ might dominate around the electron density peak during the day. The latter ion has a stronger diurnal variation due to fast dissociative recombination. *Moore et al.* [2004] calculated diurnal electron density peaks and heights for all latitudes, different seasons as well as with and without shadowing of

[1]Space Research Institute, Austrian Academy of Sciences, Graz, Austria.
[2]Department of Physics and Astronomy, University of Iowa, Iowa City, Iowa, USA.
[3]Observatoire de Paris, Meudon, France.
[4]Center for Space Physics, Boston University, Boston, Massachusetts, USA.
[5]Geological and Planetary Sciences, California Institute of Technology, Pasadena, California, USA.

0148-0227/11/2010JA016187

the rings. *Mendillo et al.* [2005] investigated the ring shadowing which leads to locally reduced electron densities. For conditions around equinox they found small radio frequency windows which might have played a role in the Voyager era observations. Another important process initially suggested by *Connerney and Waite* [1984] is the potential influx of water into the atmosphere from the rings and icy moons. Water provides a loss mechanism via charge exchange with protons and therefore can reduce the net electron density by converting long-lived atomic ions into short-lived molecular ions. In their model a planetwide influx of 4×10^7 water molecules cm^{-2} s^{-1} from the rings is consistent with the electron densities observed by radio occultations at dawn and dusk. However, the large dayside density still remains unexplained, and *Moore et al.* [2004] note that none of the water influx calculations can produce the large densities exceeding 10^5 cm^{-3} at noon. Using a constant influx of water, *Moore et al.* [2006] were able to satisfactorily reproduce the Cassini radio occultation measurements of *Nagy et al.* [2006] at equatorial latitudes for dawn and dusk. However, neither this model nor the *Moore et al.* [2004] model could reproduce the large local time variation of the peak electron density.

[5] The incompatibility of their model with the SED observations led *Majeed and McConnell* [1996] to question the atmospheric origin of SEDs. Similarly, *Rakov and Uman* [2003] argued that due to the lack of optical observations, SEDs do not provide convincing evidence for Saturnian lightning. This situation has changed, and the new combined Cassini imaging science subsystem (ISS) and Radio and Plasma Wave Science (RPWS) radio observations leave no doubt that SEDs are the radio signatures of lightning in Saturn's atmosphere. *Porco et al.* [2005] have first identified bright storm eruptions imaged in Saturn's "storm alley" at a planetocentric latitude of 35°S that correlated with the occurrence of SEDs. *Dyudina et al.* [2007] and *Fischer et al.* [2007] analyzed the combined ISS and RPWS observations in more detail and found a consistent longitudinal drift rate for storm clouds and SED episodes, plus a good correlation between the brightness of the storm clouds with the number of detected SEDs. Until the end of 2009, for 7 out of 9 SED storms ISS found an accompanying storm cloud at 35°S, and only for two short SED storms no corresponding cloud feature could be found. Inversely, no similar bright storm eruption was ever seen during SED inactivity. The final most convincing evidence are direct flashes of light that could be identified in nightside images of a storm cloud around Saturn's equinox in August 2009 [*Dyudina et al.*, 2010]. The reduced ring shine finally allowed this first visible detection of Saturn lightning, whose source should be located 125–250 km below the cloud tops most probably in the water ice cloud.

[6] An equatorial storm extending over 60° in longitude as suggested by *Kaiser et al.* [1983] for the source of SEDs could not be identified in the Voyager images. Strangely enough, *Hunt et al.* [1982] and *Sromovsky et al.* [1983] found a convective cloud feature at 35°N in the Voyager 1 as well as Voyager 2 images, respectively. This stormy feature looks very similar to the cloud features identified by Cassini ISS at the latitude of 35°S. This leads to the interesting question if the observed SEDs did come from this cloud. Since the recurrence period of the Voyager SED episodes of about 10 h 10 min. is not consistent with the rotation period of the atmosphere at 35°N, this convective cloud feature was never considered as a potential source of SEDs. Similarly, the potential 60° longitudinal extension of the storm could also be explained by the so-called over-horizon effect [*Zarka et al.*, 2006]. Parallel observations by the Cassini camera and the RPWS instrument clearly revealed that there must be radio wave propagation below the ionosphere beyond the geometrical horizon and a subsequent transmission through the ionosphere within the horizon. A closer reexamination of the old Voyager SED data would help to answer these open questions, but this would be the subject of another paper.

[7] In section 2 of this paper we will show typical SED episodes recorded by RPWS at Saturn's night and dayside. This should illustrate the technique of low-frequency cutoff measurements. In section 3 we will give the time and geometry of measurements and display selected profiles of peak electron density versus local time. Furthermore, we will also calculate average profiles in this section that will be further discussed in section 4. In this section we will also compare our measurements to midlatitude radio occultation measurements and show a correlation between Saturn ionospheric electron densities and the solar EUV (extreme ultraviolet) flux.

2. Measurement Technique

[8] The SEDs are recorded by the high-frequency receiver (HFR) of the Cassini RPWS instrument [*Gurnett et al.*, 2004]. There are two bands named HF1 and HF2 covering a frequency range of 325 kHz to 16 MHz which are relevant for SED detection, since no SEDs were detected at lower frequencies. In those two bands the receiver sweeps through the frequency range typically within a few seconds and with an instantaneous bandwidth of 25 kHz. There are different receiver modes, and the receiver can be programmed to use different frequency step sizes and integration times. In the most common survey mode HF1 covers a frequency range of 325–1800 kHz with frequency steps of 25 kHz, and HF2 covers 1825–16025 kHz with steps of 100 kHz. In the so-called direction finding (DF) mode [see, e.g., *Cecconi and Zarka*, 2005] HF1 mostly goes from 325 to 4075 kHz with a step size of 50 kHz, and HF2 sweeps from 4025 to 16025 kHz in 200 kHz steps. The DF mode comprises cross-correlation measurements between various antenna pairs to derive the incoming wave vector.

[9] Figure 1 shows an SED episode in a dynamic spectrum that displays the color-coded intensity of the radio emission (in dB relative to the background intensity) as a function of frequency (from 500 kHz to 16 MHz in a logarithmic scale) and time (over 7.5 h). The SEDs appear as narrow-banded bursts due to the sweeping nature of the receiver and the fact that they are short-lived bursts. The patchy emission below ~700 kHz is Saturn kilometric radiation (SKR). The two different modes mentioned in the previous paragraph can be clearly seen in this spectrum: For the first 3 h from 20:00 to 23:00 spacecraft event time (SCET) the DF mode is used which shows some interferences from 6 to 13 MHz. After that the survey mode is employed which shows interferences at multiples of

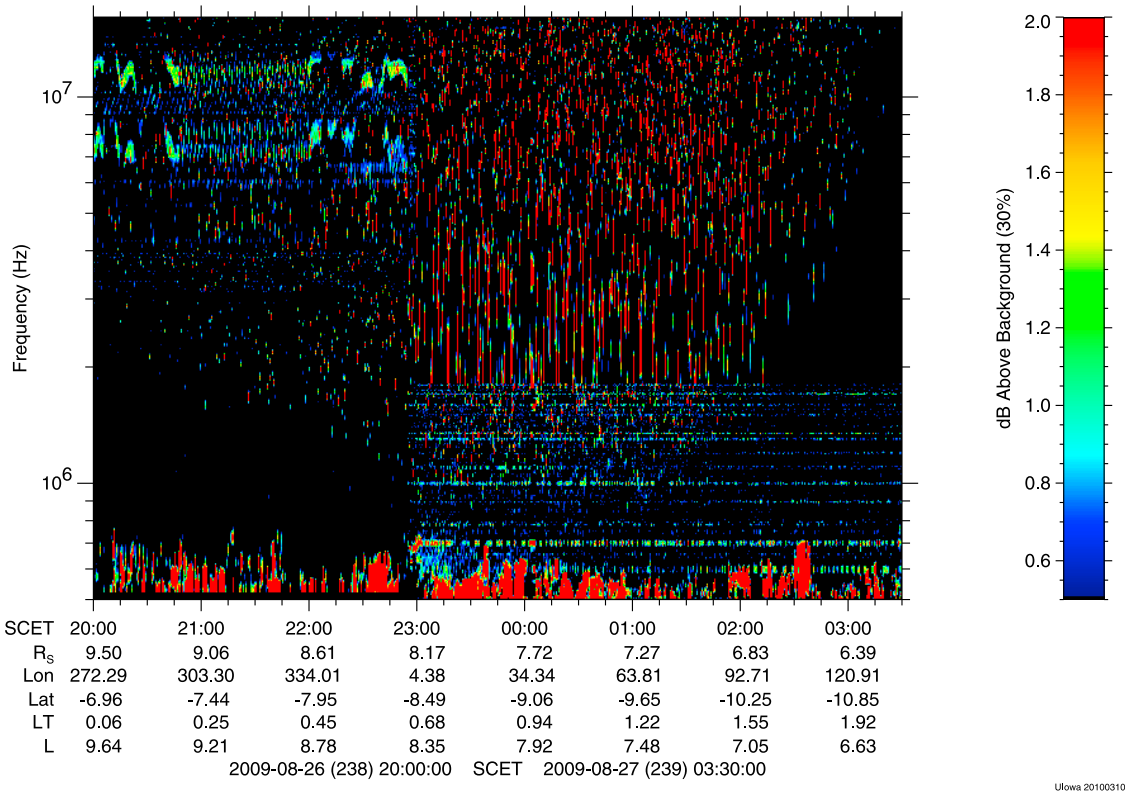

Figure 1. Dynamic spectrum of an SED episode observed by Cassini RPWS on 26–27 August 2009 from Saturn's nightside. In addition to the spacecraft event time (SCET), the radial distance, western longitude (SLS), latitude, local time, and L shell of Cassini are also indicated along the abscissa.

100 kHz in the HF1 band up to 1800 kHz, while this band is interference-free in the DF mode. However, none of these interferences hamper the ability of the receiver to detect strong SED bursts. Note that the different vertical extensions of the SEDs are mostly due to the different frequency step sizes and time resolutions in the various regions of the spectrum plus the distorting effect of the logarithmic display. From 2 to 4 MHz the SEDs should on average appear about 16 times longer in the survey mode since here the receiver makes steps of 200 kHz (not 100 kHz as usual) every 40 ms, while in the DF mode there are 50 kHz steps every 160 ms; that is, a frequency range of 200 kHz is swept through in 640 ms. This SED episode comprises 3994 SEDs, and on the abscissa it is indicated that Cassini was located on the nightside around 01 local time (LT). It can be seen relatively well that the SEDs go down to a frequency of ~900 kHz.

[10] Figure 2 shows another SED episode in a dynamic spectrum, but this time Cassini observed it from the dayside and was located around local noon. Again, the patchy emission up to ~900 kHz is SKR, and here the receiver is in the survey mode. The SED episode goes from 17:43 to 22:52 SCET and contains 1978 SEDs. The remarkable difference to Figure 1 is the low-frequency cutoff of the SEDs, which is at much higher frequencies from ~6–8 MHz. We have indicated this cutoff by a white line in Figure 2. It can be seen that the exact drawing of this line is somewhat subjective, but this uncertainty will be included by attributing a relative error of 20% to f_{cutoff}. The alert reader might also see a few bursts from ~2–3 MHz in Figure 2 (very hard to see in the printed version). Most of them are very weak and close to the SED detection threshold of 0.8 dB in this mode, which corresponds to a 4σ-threshold [*Fischer et al.*, 2006] with σ as the background fluctuation (standard deviation). There is also one stronger burst around 20:15 SCET and 2.6 MHz with an intensity of 1.6 dB above the background. There are two possible interpretations for these bursts: First, they are really SEDs and their transmission through Saturn's ionosphere might be caused by temporal and/or spatial irregularities in Saturn's ionosphere in which the electrons are slightly depleted. Second, they could be just spacecraft interferences with no further physical meaning. We note that the vast majority of SEDs are above the drawn low-frequency cutoff line. Given that lightning on Saturn is a random process, the SEDs should be randomly distributed above this line; that is, there should be no larger empty regions with no SEDs in the dynamic spectrum above it. It is also obvious that a relatively high level of SED activity is necessary to draw a proper low-frequency cutoff line f_{cutoff}. Typically, only SED episodes with more than ~300–400 SEDs are used in the analysis and all others have to be discarded.

[11] The calculation of the peak electron plasma frequency $f_{pe,peak}$ from the measurement of the cutoff frequency f_{cutoff} can now be done with a simple formula that has to include the observational geometry between the SED

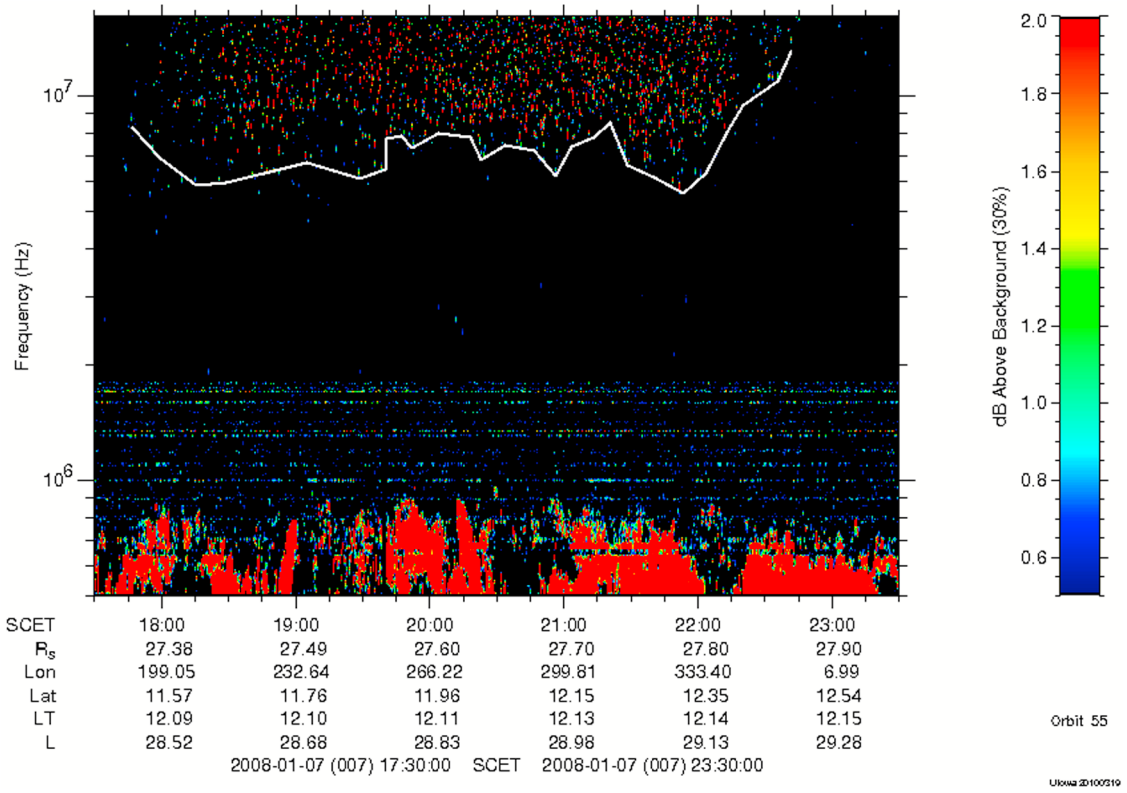

Figure 2. Dynamic spectrum of an SED episode observed by Cassini RPWS on 7 January 2008 from Saturn's dayside. Figure 2 has the same format as Figure 1, and the white line indicates the low-frequency cutoff f_{cutoff}.

storm and the observer. This has already been described in some detail by *Fischer et al.* [2007], but we shortly repeat the most important facts here. The main formula is

$$f_{pe,peak}(t) = f_{cutoff}(t)\cos[\alpha(t)], \tag{1}$$

where α is the angle between the local zenith (normal to a horizontally stratified ionosphere) and the vector from the SED storm to Cassini which we call angle of incidence. Equation (1) is a form of the so-called secant law [*Davies*, 1990] describing the relationship between an obliquely reflected wave with a frequency of f_{cutoff} and the equivalent vertical frequency corresponding to $f_{pe,peak}$. It states that based on Martyn's theorem [*Martyn*, 1935] an ionosphere can reflect (and cut off) much higher frequencies with oblique propagation than with vertical propagation. We note that for the calculation of α we take into account the oblateness of Saturn, and we use R_{po} = 54,364 km and R_{eq} = 60,268 km as polar and equatorial Saturn radius, respectively (1-bar level of *Lindal et al.* [1985]). At the planetocentric or kronocentric latitude of 35°S the angle between the local zenith and the radius vector is ~5.7°, which corresponds to the difference in kronocentric to kronodetic latitude. This shows that it is necessary to take this into account for SED storms located in the storm alley. We assume straight line propagation of the radio wave from the SED storm to Cassini and to avoid refraction effects close to grazing incidence we evaluate the equation above only at those times where $\alpha < 60°$.

[12] All three quantities in equation (1) change with observation time t during which the SED storm traverses from the west to the east with Saturn's fast atmospheric rotation under a nearly quasi-stationary spacecraft. This temporal dependence can be converted into a spatial dependence by attributing the local time of the SED storm LT_{storm} to a certain time t by using the equation

$$LT_{storm}(t) = LT_{Cas}(t) + [\lambda_{Cas}(t) - \lambda_{storm}(t)]\frac{1}{15°}. \tag{2}$$

Here LT_{Cas} and λ_{Cas} are the local time and subspacecraft western longitude of Cassini (Voyager SLS) which are known from ephemeris data. The western longitude of the storm λ_{storm} is only slightly changing with time (typically a fraction of a degree per Earth day), and in section 3 we will give the relations for $\lambda_{storm} = \lambda_{storm}(t)$ for all observed SED storms which come from imaging observations of the associated storm clouds. Usually the storm has a longitudinal extension around 3°, and λ_{storm} should be the longitude of its center.

[13] The peak electron plasma frequency $f_{pe,peak}$ can simply be converted to the peak electron density N_e by using the equation

$$N_e = \frac{4\pi^2 m_e \varepsilon_0}{e^2} f_{pe,peak}^2, \tag{3}$$

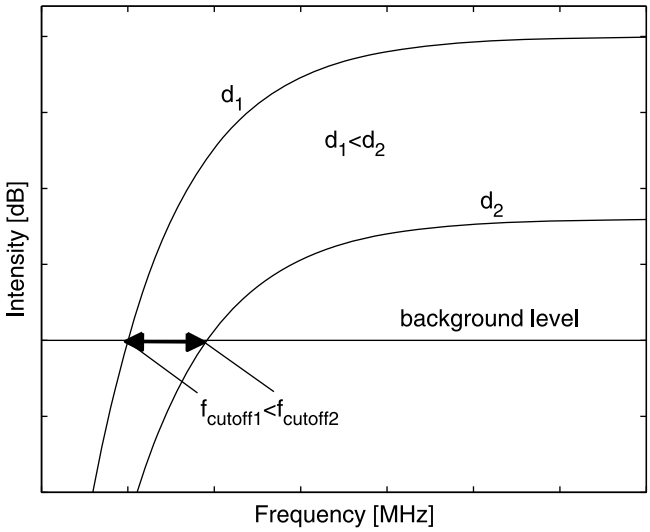

Figure 3. Illustration of the effect of distance d on the cutoff frequency f_{cutoff}. The intensity of the SEDs in dB above the background level is plotted in an arbitrary scale versus frequency. A closer observer with $d_1 < d_2$ results in a lower cutoff frequency with $f_{cutoff1} < f_{cutoff2}$.

with m_e as the electron mass, ε_0 as the permittivity of free space, and e as the elementary charge. One can also simply use the well-known numerical formula of $N_e = f^2_{pe,peak}/81$ where N_e is in electrons per cm^3 when $f_{pe,peak}$ is inserted in kHz.

[14] In summary, the above equations are used to calculate a peak electron density profile $N_e = N_e(LT_{storm})$ as a function of local time of the storm for an SED episode. From the measured cutoff frequency f_{cutoff} and the calculated angle of incidence α we can calculate the peak plasma frequency $f_{pe,peak}$ with equation (1), which is transferred to the peak electron density via equation (3). These calculations are first done as a function of time t which using equation (2) can be converted into a local time LT_{storm} of the SED storm to gain the profile $N_e = N_e(LT_{storm})$.

[15] To a certain degree the cutoff frequency on a spectrogram also depends on the SED intensity which is mainly related to the distance d of Cassini to Saturn. The SED power spectrum was found to be nearly flat in the frequency range of 2–16 MHz [*Zarka et al.*, 2006]. However, the SED power versus frequency is not exactly a step function, but shows a progressive attenuation with decreasing frequency close to the cutoff. If the observation point is moved closer to the SED storm, the intensity increase with $1/d^2$ will thus allow the observer to detect weaker bursts at lower frequencies. This is illustrated in Figure 3 for two SED episodes where a closer spacecraft with $d_1 < d_2$ results in a lower cutoff frequency with $f_{cutoff1} < f_{cutoff2}$. We will investigate this effect by grouping the electron density profiles with respect to spacecraft distance.

[16] We make a quick estimate of the ratio between the electron densities of Saturn's nightside and dayside by using Figures 1 and 2. A geometrical calculation for the nightside episode of Figure 1 shows that $\alpha = 44°$ for day of year (DOY) 239, 2009, 00:00 SCET, and that the SED storm is around ~03 LT. Similarly, for the dayside episode of Figure 2 α has the same value of 44° on DOY 007, 2008, 20:30 SCET, and the storm is approximately at noon. The cutoff frequencies for these two points in time are ~1 MHz for the nightside and ~7 MHz for the dayside episode, respectively. Since the geometries are such that the angle α is practically the same for both cases, the ratio between the electron densities is simply given by the ratio of the squared cutoff frequencies which is $7^2 = 49$. This quick first estimate gives us a typical value for the diurnal variation in peak electron density of 1 to 2 orders of magnitude, which we will find in section 3.

3. Results

3.1. Occurrence and Observational Geometry of SED Storms

[17] Until the end of the year 2009 there were nine SED storms that lasted from a few days up to several months. There was one weak SED storm before Cassini's Saturn Orbit Insertion named storm 0, there were three other storms A, B, and C in 2004, one SED storm D in 2005, one storm E in early 2006, a 7.5 monthlong SED storm F from the end of 2007 until mid 2008, one SED storm G at the end of 2008, and finally SED storm H lasted for about 11 months throughout 2009 with some weeklong interruptions. For only two weak and short storms, namely storm 0 of May 2004 and storm D of June 2005, the Cassini cameras did not image a related storm system. Furthermore, all the SED episodes of those two storms did not have enough SEDs to draw a clear low-frequency cutoff, hence this data cannot be used for our analysis. For all the other SED storms the Cassini camera could image SED-related cloud features at a kronocentric

Table 1. SED Storms Used for the Analysis of Peak Electron Densities[a]

Name of SED Storm	Time Interval	Cassini Local Time	SED Storm Longitude (Voyager SLS)	Number of Profiles
ABC	13 Jul to 28 Sep 2004	5.1–6.5	$\lambda_{ABC}[°] = 222.2 + 0.30\ t_{DOY}$	5
E	23 Jan to 23 Feb 2006	3.1–8.5	$\lambda_E[°] = 155.1 + 0.61\ t_{DOY}$	29
F[1]	27 Nov 2007 to 10 Mar 2008	all	$\lambda_{F^1}[°] = 173.2 + 0.30\ t_{DOY}$	33
F[2]	11 Mar to 15 Jul 2008	all	$\lambda_{F^2}[°] = 268.0 + 0.34\ t_{DOY}$	53
G	19 Nov to 11 Dec 2008	all	$\lambda_G[°] = 218.0 + 0.30\ t_{DOY}$	11
H	14 Jan to 13 Dec 2009	all	$\lambda_H[°] = 320.0 + 0.22\ t_{DOY}$	100

[a]We list the name of the SED storm and its time interval (day, month, and year from the beginning to the end), the local time range of Cassini, the longitude of the SED storm, and the number of electron density profiles that were gained from each storm. The longitudes λ of the SED storms are western longitudes in degrees in the Voyager SLS system, and the time t_{DOY} has to be inserted as DOY when the storm started. For SED storm F[1] t_{DOY} has to be inserted as DOY 2007, whereas for F[2] it is the DOY 2008. The last column shows the number of profiles that were used for the calculation of the average storm profile, and the total number of these profiles is 231.

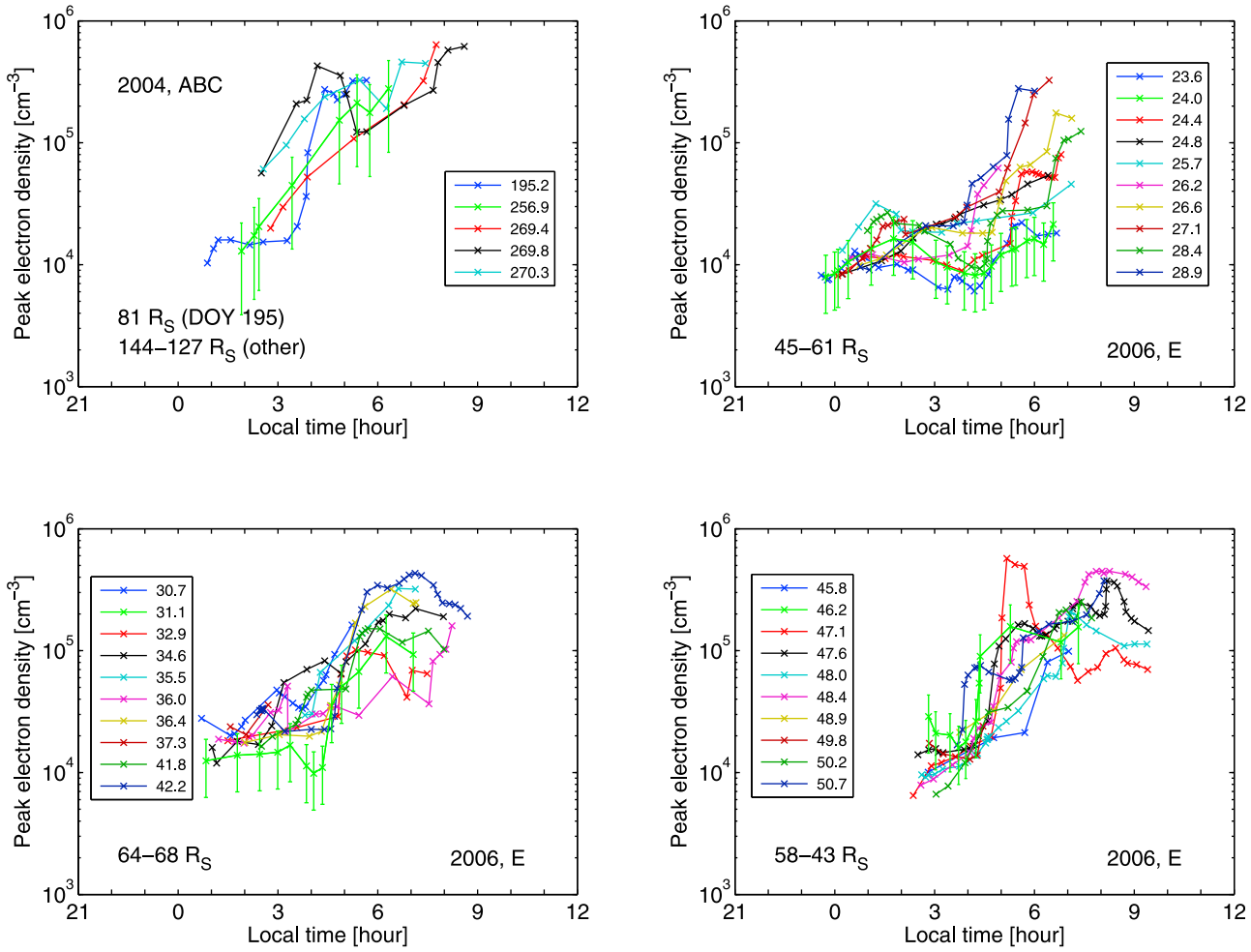

Figure 4. Profiles of peak electron density versus local time for Saturn's ionosphere at a planetocentric latitude of 35°S. (top left) Five single profiles are shown from the SED storms ABC from summer 2004 and (top right, bottom left, and bottom right) display 30 profiles from SED storm E of early 2006. The numbers in the legends indicate the approximate time of the center of the respective SED episode in days of the year. One can see the range of spacecraft distances in Saturn radii (R_S) for each panel.

latitude of 35°S. In the following Table 1 we list all the SED storms used for our analysis with various other information like the time when they happened, the local time range of Cassini, the longitude of the SED storm and the number of SED episodes that could be used to determine an electron density profile $N_e = N_e(LT_{storm})$.

[18] Storms A, B, and C were put together in one line in Table 1 since they actually all belonged to the same storm system that waxed and waned in intensity with two week-long interruptions. The longitudes of the various SED storms were derived from images taken by the Cassini camera as well as ground-based telescopic observations from Earth by amateurs. All the storms showed a slight drift to the west (from ~0.2° to ~0.6° per Earth day) and the longitudinal position was approximated by a linear fit. Storm F is divided into two parts: The first part F[1] until early March 2008 is characterized by a single storm that drifted at a rate of approximately 0.3° per Earth day. From 6 March until 10 March the RPWS recorded uninterrupted SED activity for 9 consecutive Saturn rotations which only can be explained by the presence of at least a second storm system. This was a unique event since normally the SED activity is organized in episodes with gaps in SED activity when the storm is located beyond the radio horizon on the far side of the planet as seen from Cassini. After those 9 Saturn rotations the typical episodic behavior continued, but the longitude range at which SED activity was recorded seemed somewhat larger than usual. Ground-based optical observations by amateurs as well as Cassini ISS observations somewhat later revealed the cause of this behavior, which was that starting in mid-March 2008 there were two SED storm systems present at the same latitude of 35°S separated by ~30° in longitude. *Delcroix and Fischer* [2010] show that the drift of these two systems is similar to the average value of 0.34° per Earth day. The presence of two storm systems complicates our analysis since we cannot tell exactly where the SEDs originate that form the low-frequency cutoff. However, since the longitudinal separation was only about 2 h in local time, we decided to perform the analysis as described above and substituted the two real

storms by a hypothetical one which we placed exactly in the middle of them. The longitudinal position of this hypothetical storm F^2 is given as a function of time in Table 1. It was used to calculate the angle of incidence α which now has a larger error than in the usual case with just one storm system. Intriguing images of the two bright cloud features were captured by Chris Go on 1 May (see http://saturn.cstoneind.com/) and by Cassini ISS on 18 June 2008.

3.2. Single Electron Density Profiles

[19] In this subsection we will show most of the peak electron density profiles $N_e = N_e(LT_{storm})$ derived from single SED episodes. The SED storms A, B, and C from 2004 comprised 80 episodes in total [*Fischer et al.*, 2006], but only 5 of them had enough SEDs to derive the density profiles which are shown in Figure 4 (top left). Those 5 SED episodes had slightly more than 300 SEDs each, which is just barely enough to draw a reasonable low-frequency profile. The other three panels of Figure 4 show a total of 30 profiles from the SED storm E of early 2006 which consisted of 71 SED episodes in total. Two of these profiles were already shown and analyzed by *Fischer et al.* [2007], namely the episodes E2 centered around DOY 24.0 and E56 around DOY 48.0, 2006. In all profiles in this subsection we indicate the SED episodes by numbers in the legends of Figures 4, 5, 6, and 7 which give the fractions of the day of year of the approximate center time of the respective episode. Furthermore, we draw error bars for just one profile (the green one) in each panel to avoid confusion among the multiple profiles. The size of the error bars usually corresponds to a relative error of 50%. We attribute 20% of the error to the measurement uncertainty of the low-frequency cutoff and 5% to the geometric uncertainty in the angle of incidence α. Assuming that the relative errors add up, we have 25% error for the peak electron plasma frequency. The relative error for the electron density N_e is twice of that since in equation (3) N_e is calculated from the square of the peak electron plasma frequency. These error estimates would, e.g., mean an absolute error of $\Delta f_{cutoff} =$ 400 kHz for a typical cutoff at $f_{cutoff} = 2$ MHz and a $\Delta\alpha \approx 3°$ error for $\alpha \approx 45°$. For the HF2 part of the receiver 400 kHz usually correspond to 2 or 4 times the frequency resolution. At lower frequencies in the HF1 band the frequency resolution is better and usually 25 kHz. The low-frequency cutoff line as drawn in Figure 2 consists of discrete measurement points that were set manually in approximately equal intervals of time (and local time) in the spectrogram. These measurements are somewhat subjective and might be less precise at higher frequencies since we used logarithmic spectrograms. Therefore, we introduced the percentage error to account for higher errors at higher frequencies and lower errors at lower frequencies. The error in the local time of the storm comes from the error in the optical storm observation. The drift of the storms in longitude was approximated with a linear fit (see Table 1), and the jitter of measurement points around this fitting line is typically about ±5° in longitude corresponding to an error of ±0.3 h in local time (not drawn in all the profiles). For the SED episodes of the storms A, B, and C we increased the error of the low-frequency cutoff measurement to 30% due to the low number of SEDs to arrive at a total relative error of 70% for N_e.

[20] The profiles in Figure 4 show only electron densities around dawn due to the local time position of the Cassini spacecraft as given in Table 1. The profiles largely reflect the rise in electron density when the SED storm traverses from the nightside to the dayside. For storms A, B, and C this rise starts relatively early around 03–04 LT. The local sunrise at the southern latitude of 35°S took place around 5.1 LT in southern summer conditions like Saturn was in 2004. This was valid for the surface, but for an altitude of the ionosphere of 2000 km the sunrise shifts by about 1 h to an earlier local time. It can be seen that about 1.5 years later in early 2006 this rise has shifted to somewhat later local times for SED storm E (local sunrise around 5.5 LT on the surface). Another interesting feature can be seen in Figure 4 (top right). For some profiles there seems to be a local minimum in electron density around 03–05 LT which was later also found for SED storm H. During the early phase of SED storm E the spacecraft was in an optimal position to sample those subspacecraft local times. Later the spacecraft moved to late morning local times, but in some profiles this local minimum can still be seen. An exceptional profile is plotted as the red line in Figure 4 (bottom right) (from the SED episode centered on DOY 47.1, 2006). We specifically looked at this SED episode with the curious peak at 05–06 LT, and it consisted of 1853 SEDs and seemed to show a reliable low-frequency cutoff with a clear bite-out. Hence, the profile is most likely real, and it might display a time-variable and localized phenomenon resulting in this curious increase in electron density. Electron densities are somewhat higher for the storms A, B, and C compared to storm E. This could be due to different solar conditions, or there is a small systematic influence of the spacecraft distance.

[21] We continue by showing all the profiles retrieved from the first part of SED storm F, named F^1, from the end of November 2007 until early March 2008 in Figure 5 which exhibit a good coverage of the local times around noon. It can be seen that for most profiles the peak electron density is somewhat above 10^5 cm^{-3} around noon. Although Cassini made several orbits during this time, we could not retrieve any reliable nightside profiles. The short-time periapsis passes of Cassini close to midnight brought no results due to at least one of the following 3 reasons. First, there was either low SED activity when Cassini traversed the nightside or second, the SED storm was out of phase, i.e., not at the nightside during this short time resulting in $\alpha > 60°$. And third, it also happened that the low-frequency cutoff was obscured by SKR around 800 kHz.

[22] Figure 5 (bottom right) shows the profiles retrieved from a close distance of the spacecraft ranging from 6–14 R_S (Saturn radii). In contrast to the other panels the local time coverage is better and there seems to be more variation between the various profiles. There is one exceptional profile retrieved on DOY 62, 2008 (yellow line), that stays at the constant low level of ~10^4 cm^{-3} also on the dayside. A potential explanation for this could be a second storm system that is still located on the nightside and therefore has SEDs that still go down to lower frequencies. This episode took place just 4 days before the uninterrupted SED activity from 6–10 March, and so it is very likely that one of the other storms already showed up here for the first time.

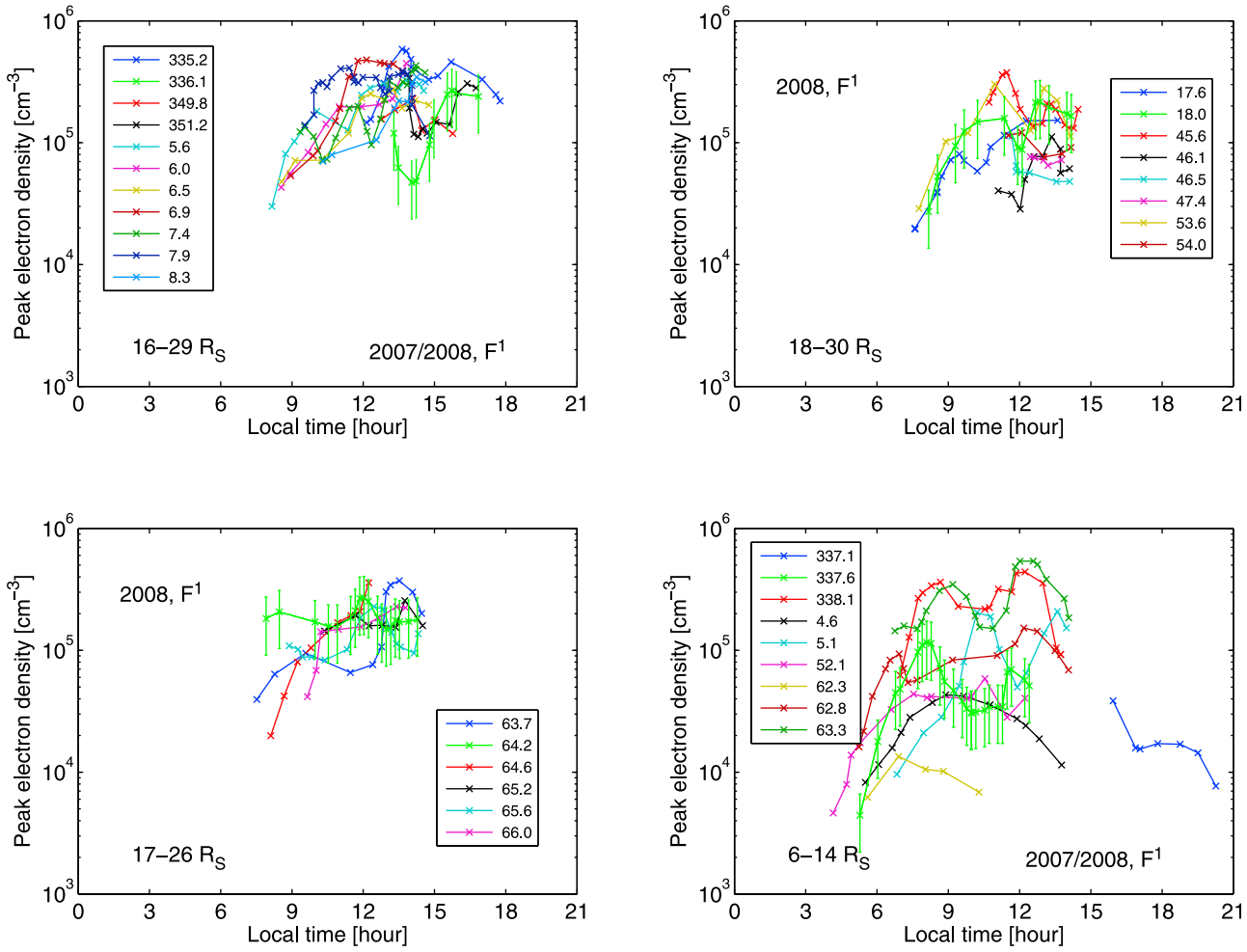

Figure 5. Profiles of peak electron density versus local time for Saturn's ionosphere at a planetocentric latitude of 35°S. There are 34 profiles from SED storm F^1 on display, and like Figure 4, the numbers in the legends indicate the approximate time of the center of the respective SED episode in days of the year (days greater than 330 are from the year 2007). In the lower left corner of each panel one can see the range of spacecraft distances in Saturn radii.

[23] Three panels of Figure 6 show profiles that were retrieved from SED storm F^2 from March until July 2008. As described earlier, imaging observations showed two cloud features separated by ~30° in longitude which we approximate by a single storm located in the middle of them. This increases the error in local time to ±1.3 h (not drawn). To account for the higher uncertainty in α we increased the total relative error of the electron density to 60%. Figure 6 (top) shows 20 reliable profiles (out of 53), which are relatively similar to the profiles gained during storm F^1 with an electron density above 10^5 cm^{-3} for most profiles at noon. They are grouped after spacecraft distance with 6–16 R_S (Figure 6, top left) and 17–24 R_S (Figure 6, top right). Here the distance effect seems marginal and electron densities are only slightly higher for larger distances. For illustration we also show 8 unreliable profiles from storm F^2 in Figure 6 (bottom left). The first 4 of them were recorded during the uninterrupted SED activity from 6–10 March 2008. Cassini was located around noon and seems to have retrieved reasonable electron densities. However, we cannot be sure about the position of additional sources and the two sources separated by 2 h in local time are actually not enough to explain the permanent SED activity. At least 3 or maybe even more SED sources were active during this peculiar period as shown by *Delcroix and Fischer* [2010] from observations by ground-based telescopes. Like for SED storm F^1, no reliable profiles could be retrieved for the nightside during F^2 due to the same reasons as mentioned above. The 4 other profiles of Figure 6 (bottom left) show some of these unreliable nightside profiles. The main difficulty with them was the presence of SKR, so the real low-frequency cutoff could in fact be lower. Furthermore, the close distance of Cassini while it was on the nightside leads to bigger errors in α when multiple sources are present. For example, the late rise in electron density of the cyan profile (from DOY 93.0, 2008) could be due to such an effect. Figure 6 (bottom right) shows 11 reliable profiles from SED storm G in late 2008. Only one of them shows an electron density for the nightside with values around 10^4 cm^{-3}. This profile was

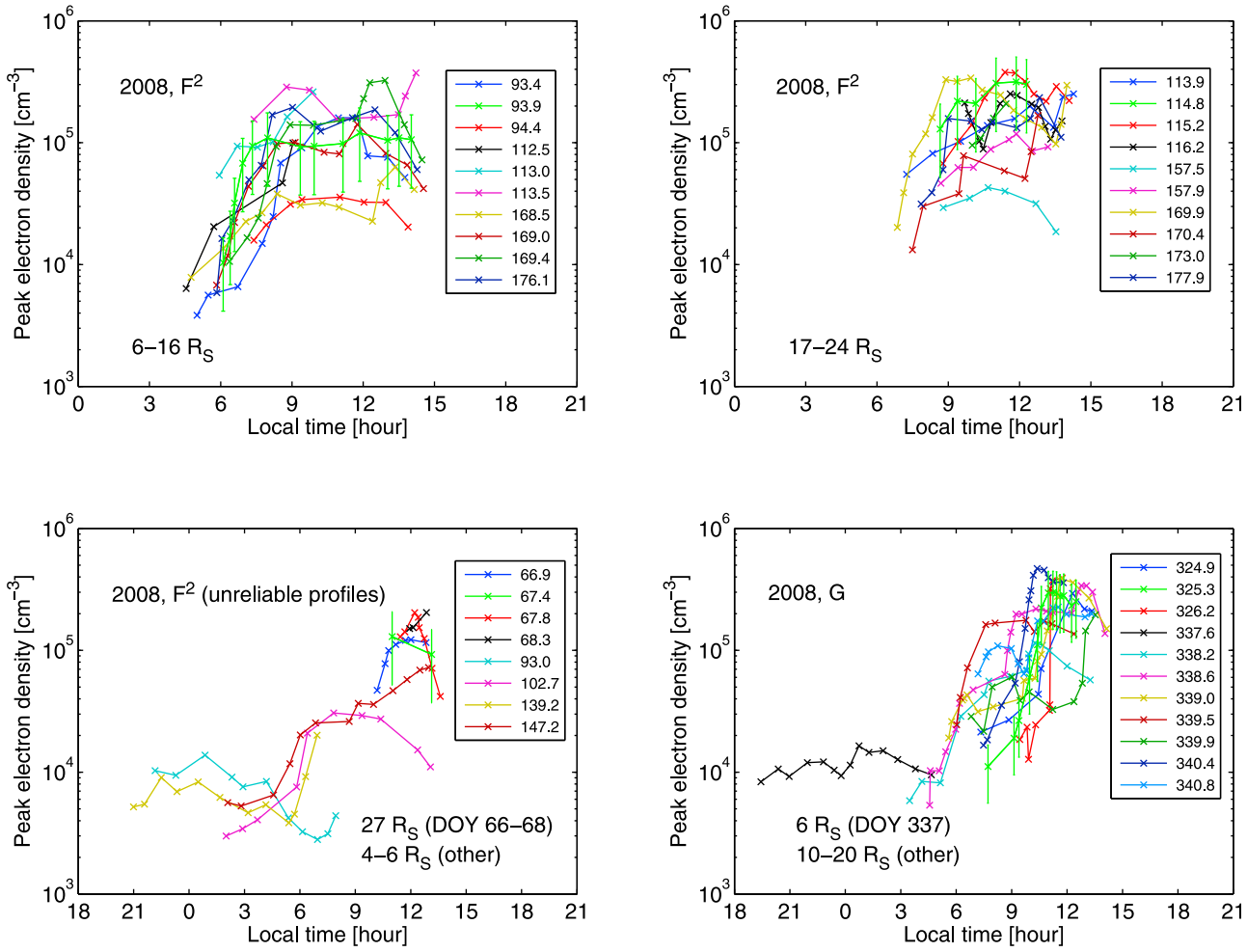

Figure 6. Profiles of peak electron density versus local time for Saturn's ionosphere at a planetocentric latitude of 35°S. (top) Twenty profiles from SED storm F^2 from March until July 2008, while (bottom left) 8 unreliable profiles are shown from the same storm for illustration. (bottom right) Eleven profiles from SED storm G of late 2008. The ranges of spacecraft distances for each subset of profiles are given in Saturn radii.

retrieved from a close distance of 6 R_S, while the distance was 10–20 R_S for the dayside profiles.

[24] Figure 7 displays 40 profiles that where retrieved throughout the year 2009 during which the SED storm H exhibited nearly 500 SED episodes in total. Many of them could be retrieved on the nightside providing a good coverage of all local times since most orbits of Cassini during 2009 had their apoapsis on the dusk side. Again, we grouped the profiles after spacecraft distance. We have medium distances of 14–20 R_S in the upper panels, and the lower panels show close distance profiles (4–10 R_S) on the left and large distance profiles (33–49 R_S) on the right side. It is remarkable that the close distance profiles show less diurnal variation. While the nightside densities are comparable with other profiles, the electron densities at noon are somewhat smaller compared to the others. Especially the close distance profiles have their minimum in electron density at the early morning side around 03–05 LT as was already mentioned for SED storm E. Such a minimum is favorable to the assumptions leading to the over-horizon effect described by *Zarka et al.* [2006]. The large distance profiles show much higher densities in the afternoon and early evening local times. In section 3.3 we will calculate average profiles for the various SED storms.

3.3. Averaged Electron Density Profiles

[25] The last column of Table 1 lists the number of profiles that were used to calculate an average profile for the respective storm. We have chosen only the reliable profiles for averaging, e.g., the ones displayed in Figure 6 (bottom left) are not included. We also excluded the exceptional profile from DOY 47.1, 2006, of SED storm E as well as the exceptional profile from storm F^1 which was retrieved around DOY 62.3, 2008. Figure 8 shows the average profiles for the storms labeled ABC, E, F^1, F^2, G, and H (see Table 1). The values of the electron density N_e of all reliable profiles were binned in 24 one-hour local time intervals and the averages and standard deviations were calculated for each 1 h bin. The standard deviations are plotted as vertical bars reflecting the variability of Saturn's ionosphere. They

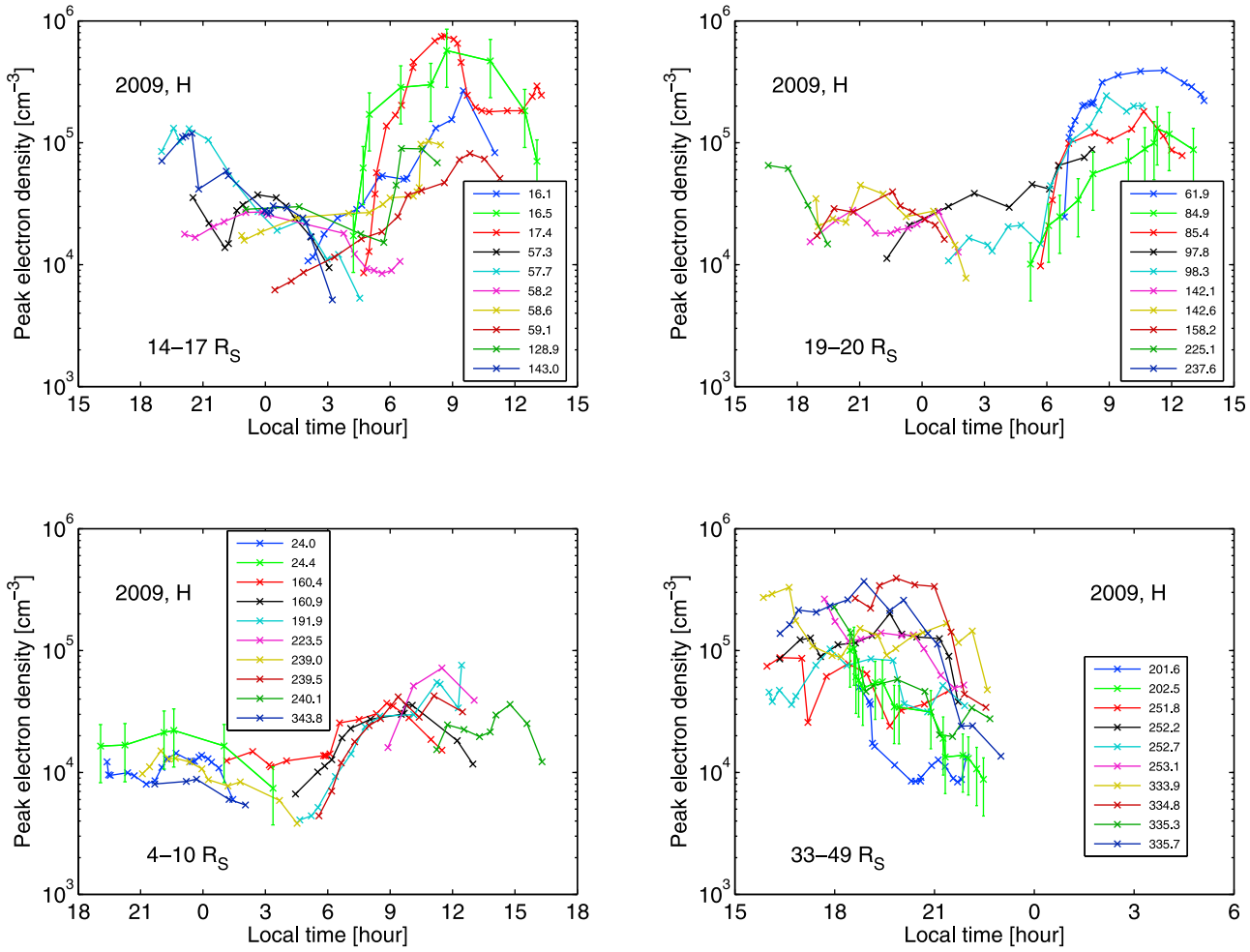

Figure 7. Profiles of peak electron density versus local time for Saturn's ionosphere at a planetocentric latitude of 35°S. A total of 4 × 10 profiles retrieved from SED storm H of 2009 is displayed in the four panels with the numbers in the legends indicating the approximate time of the center of the respective SED episode in days of the year. Selected profiles were grouped after spacecraft distance which is indicated in each panel.

should not really be interpreted as error bars like in the single profiles of section 3.2, because one can expect a seasonal variability of Saturn's ionosphere which is also influenced by the changing EUV flux from the sun. In some cases the standard deviations are bigger than the averages, and then the lower end extends down to the lowest value of the ordinate. It can be clearly seen that this is the case mostly at dawn and dusk where the variability of the electron density can be expected to be higher. The averages were calculated for 3 different threshold values of the angle of incidence α, namely $\alpha < 50°$ (plotted as circles), $\alpha < 60°$ (plotted as point with the vertical bars), and $\alpha < 70°$ (plotted as crosses).

[26] We want to point out why we chose the range of $\alpha < 60°$ for the angle of incidence. A ray tracing analysis was done by *Kaiser et al.* [1984] for Saturn's ionosphere assuming an ideal Chapman layer with a peak electron density of 10^4 cm^{-3} located 1100 km above the 1-bar level and with a 300 km scale height. This analysis has revealed little deviation from straight line propagation for radio waves with an angle of incidence of $\alpha = 60°$ close to the limiting frequency. We did not perform another ray tracing in our investigation, but tested other limits for α in the following way. The circles in Figure 8 display the averages when we limited the region of possible angles of incidence to $\alpha < 50°$, whereas for the crosses we extended the region to $\alpha < 70°$. It can be seen that there are no significant differences between those two limits and our default limit of $\alpha < 60°$, which was used in Figures 4, 5, 6, and 7 for the single profiles. The only large deviation in the interval of 18–19 LT of storm F[1] is due to the limited number of profiles. When the limit $\alpha < 50°$ is used in Figures 4, 5, 6, and 7, many single profiles are simply cut at the beginning and at the end since the minimum of α is reached at the center of each profile and larger values of α are at both ends. Similarly, many lines get extended when we take $\alpha < 70°$ and a larger local time range can be covered. However, many of those extended lines (not shown) exhibited significant drops in electron density at the edges where $60° \leq \alpha < 70°$, similar in shape to the function $\cos(\alpha)$ which is used in equation (1) for the calculation of electron density. Since these drops occurred at various local times it suggests

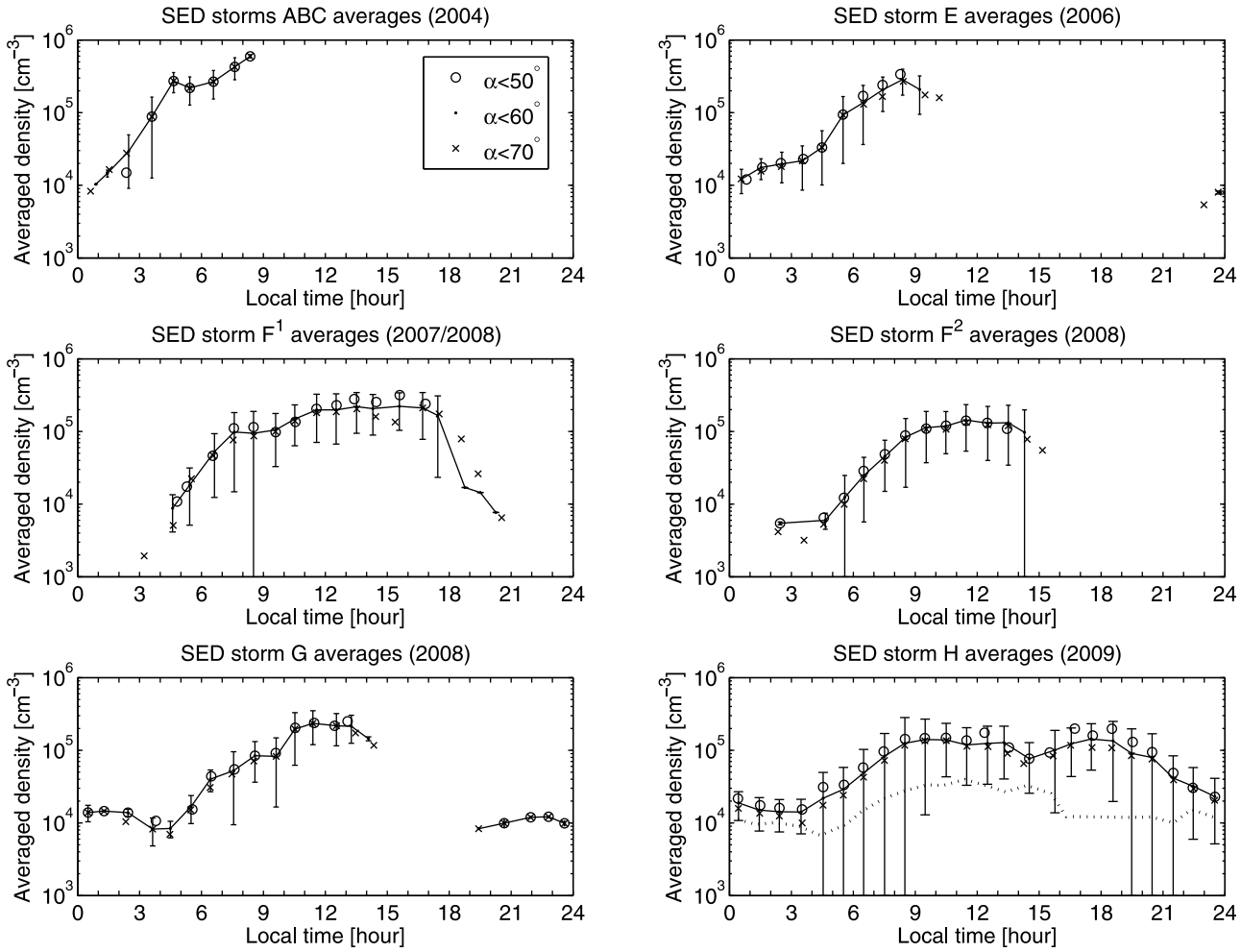

Figure 8. Averaged peak electron densities as a function of local time for each SED storm from 2004 until the end of 2009. Local time bins of 1 h were used to calculate the averages and the standard deviations (only for $\alpha < 60°$), which are drawn as vertical bars. The averages were calculated for three different sets of thresholds for the angle of incidence α as given in the legend (Figure 8, top). The dotted line (Figure 8, bottom right) is the average of 10 close distance profiles (within 10 R_S) for storm H (see Figure 7).

that due to refraction effects and due to the large gradient of the cosine function in this range of α, equation (1) cannot be used anymore to adequately describe the physical situation. The crosses describing the averages of the limit $\alpha < 70°$ in Figure 8 can usually be found at somewhat lower levels due to the drops in electron density at the episode's edges.

[27] The dotted line in Figure 8 (bottom right) shows the average electron density for the 10 close distance profiles of SED storm H that are displayed in Figure 7 (bottom left) (for $\alpha < 60°$). This profile has lower-electron densities by a factor of about 2 compared to the overall average profile.

4. Discussion

4.1. Comparison of Cassini Profiles With Respect to Solar Zenith Angle and Spacecraft Distance

[28] For comparison we plot again the average profiles (for $\alpha < 60°$) of all SED storms as a function of local time in Figure 9, but in one single diagram. Furthermore, we plot an average profile of all SED storms which is very similar to the average profile of SED storm H due to the large number of profiles for this storm. To indicate the variability of those averaged profiles we also plot those measurements within one single profile where the angle of incidence α is a minimum. This is mostly the case when the SED storm passes through the central meridian as seen from Cassini. A further restriction was $\alpha < 40°$ which reduced the number of points to 177 since for the other 54 profiles (total of 231) even the minimal angle of incidence α_{min} was $\geq 40°$. The measurements with small angles of incidence can be considered as the most reliable ones and they do group around the average curve with a certain spread due to the variability of Saturn's ionosphere. It can be seen that all measurements from about 12 to 19 LT were made with angles of incidence $40° \leq \alpha < 60°$. This is due to the orbit of Cassini which usually was at higher northern latitudes in afternoon local times during SED storms whereas the storm was always located at 35°S. Since the local time coverage of some of the storms is limited we cannot calculate a noon-to-midnight electron density ratio for all of them. Instead, we

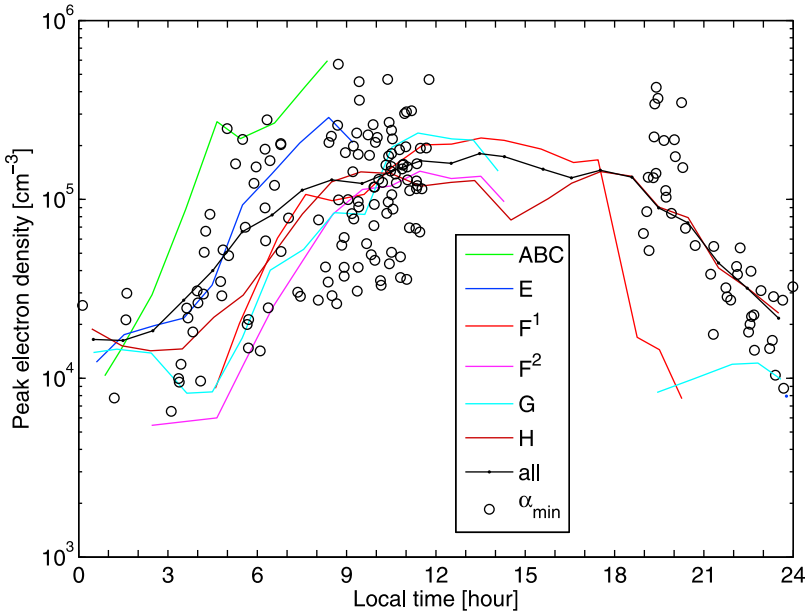

Figure 9. Peak electron densities as a function of local time for each SED storm from 2004 until the end of 2009 (storms ABC, E, F^1, F^2, G, and H see Table 1). The black line with dots gives the average curve of all profiles, averaged in local time bins of 1 h. The circles give those measurements within one SED episode where the angle of incidence α was a minimum and also <40°.

simply calculate the ratio between the maximum and the minimum peak electron density for the various SED storms. Minimum and maximum peak electron density are also not necessarily located at midnight and noon, respectively. The minimum often can be rather found early in the morning around 03–05 LT, and the maximum is sometimes at 10–11 LT. Using the average profiles of Figure 9 we obtain a maximum-to-minimum electron density ratio of 58 for SED storms ABC, 36 for E, 29 for F^1, 26 for F^2, 29 for G, and 10 for SED storm H. For the 10 close distance profiles of SED storm H this value is only 6. There seems to be a decreasing trend with time which might be linked to the low solar EUV flux in recent years.

[29] Another feature of Figure 9 is the early rise of electron density for SED storms ABC and E on the morning side compared to the other storms where the electron density usually increases significantly from 05 to 08 LT. This is partly a seasonal influence since the sun rises earlier for southern summer conditions at the southern latitude of the storm, especially when the peak layer is at high altitudes. To eliminate this seasonal effect and to show all measurement points in one figure again, we plot all electron density measurements as a function of the solar zenith angle in Figure 10. Shown are the morning side with local times from $0 < LT < 12$ (Figure 10, left) and the evening side with $12 < LT < 24$ (Figure 10, right). Solar zenith angles vary from ~20° at noon to ~150° at midnight. Electron densities retrieved from storms ABC and E (green and blue points in Figure 10 still show a shift also with respect to the solar zenith angle. This might be a systematic effect of the spacecraft distance since for storms ABC and E Cassini was beyond 43 R_S from Saturn, and measurements from large distances result in cutoffs at higher frequencies since the bursts get extraordinarily weak and blend into the background.

[30] Figure 11 was plotted to investigate the influence of the radial distance of the spacecraft as it was mentioned toward the end of section 2. We display the discrete measurement points in different colors for several distance intervals as a function of local time. Shown are close distances from below 5–14 R_S in 4 intervals (Figure 11, left) and larger distances beyond 14 R_S in 5 intervals (Figure 11, right). There are remarkable differences between those two panels. The close distance measurements show less spread in density and a clear minimum around 04–05 LT is present. This minimum is absent for measurements from a larger distance. Among the larger distances the blue and black points denote measurements in the interval 45–80 R_S and beyond 80 R_S, respectively. Also those measurements usually show higher densities than the red, green, and magenta points from 14–45 R_S. Hence, there is a certain systematic influence of the spacecraft distance on the electron density measurements. It is not very dramatic, but clearly present and typically the density values are somewhat smaller for closer distances. We plotted the average of all measurements within 14 R_S as solid line (Figure 11, left) and also plotted the average of all measurements beyond 14 R_S as dotted line. The difference in electron densities is typically a factor of 2 except for midnight where the values are similar and the early morning minimum where the difference is larger. The minimum in the afternoon for close distance measurements is not reliable due to the small number of points. The distance effect is even more pronounced for very close distances within 7 R_S (red and green points in Figure 11 (left)), that show noon densities below 10^5 cm^{-3} but also early morning minimums down to 4×10^3 cm^{-3}. The ratio between minimum and maximum densities seems to be less sensitive, and it is typically 1 to 2 orders of magnitude.

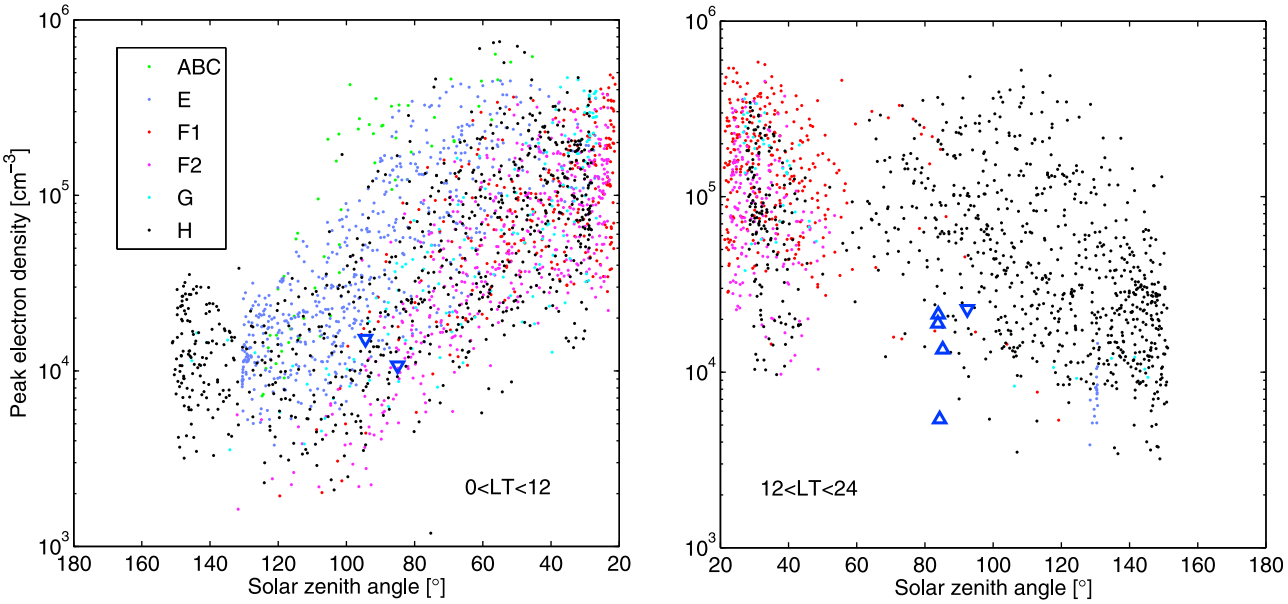

Figure 10. All peak electron density measurements as a function of solar zenith angle for each SED storm from 2004 until the end of 2009 (storms ABC, E, F^1, F^2, G, and H see Table 1). (left) The morning side (local times from 0 to 12 h) and (right) the evening side (from 12 to 24 h). The blue triangles show the results of the midlatitude radio occultation measurements by *Kliore et al.* [2009]. Four of them point upward to indicate measurements from the northern hemisphere, and three of them point downward for southern hemisphere measurements.

4.2. Comparison to Voyager Measurements and Radio Occultations

[31] Comparing our profiles in Figure 9 or Figure 11 to the profile gained by Voyager 1 [*Kaiser et al.*, 1984, Figure 4] we find that the diurnal variation in electron density was larger for Voyager with a mean day-night density ratio of about 150. The Voyager measurements were not only made at the closest approach episode, but also at the SED episodes

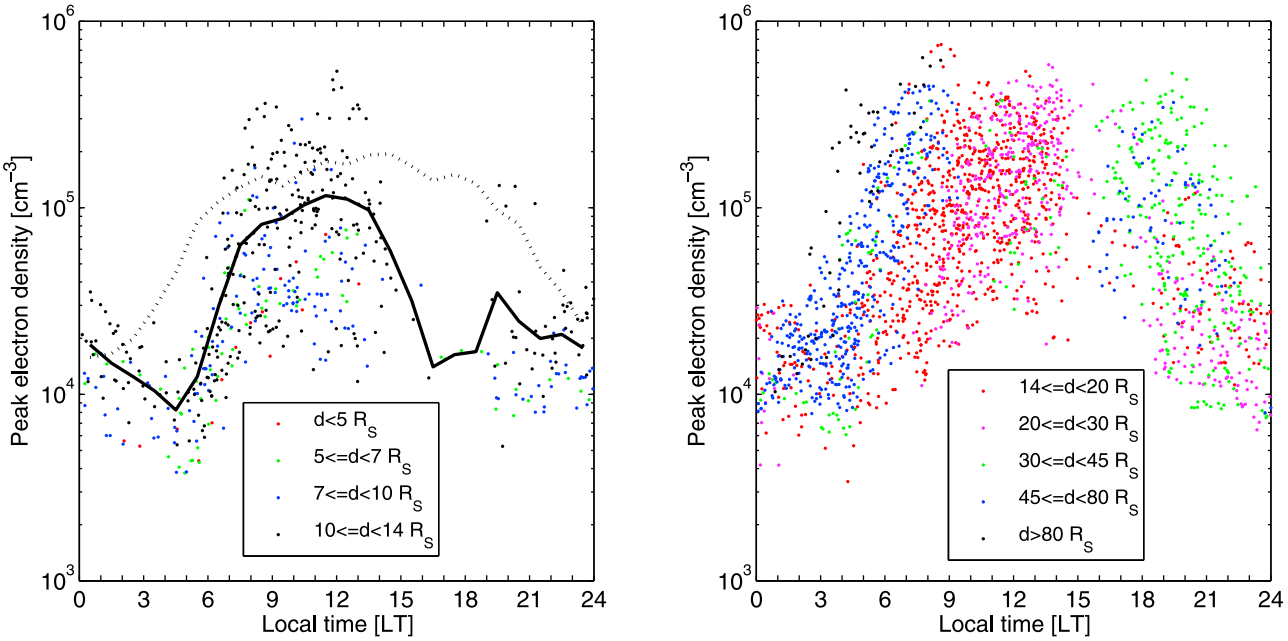

Figure 11. All peak electron density measurements as a function of local time and grouped by spacecraft distances in Saturn radii. Data retrieved from 2004–2009 for Saturn's ionosphere at a planetocentric latitude of 35°S. The solid line shows the average of measurements within 14 R_S, and the dotted line is the average of points beyond 14 R_S.

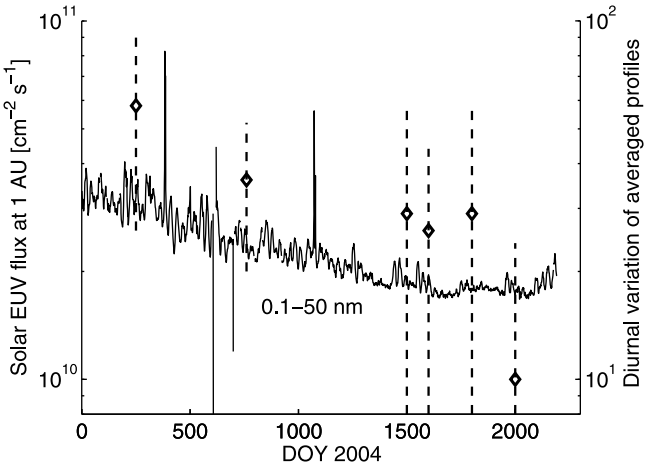

Figure 12. Solar EUV flux as measured by SEM/SOHO at 1 AU and diurnal variation in peak electron density displayed on a common abscissa which is the time in days of the year 2004. The line indicates the daily averages of the solar EUV flux from 0.1 to 50 nm, and the corresponding ordinate is on the left-hand side. The diamonds give the ratio between the maximum and minimum electron densities of the averaged profiles displayed in Figure 9, and the dashed lines are the error bars. The corresponding ordinate is on the right-hand side and the six diamonds (for SED storms ABC, E, F^1, F^2, G, and H) are placed approximately in the temporal center of each storm.

preceding and following the closest approach. The high densities at the dayside were actually measured by Voyager 1 from distances of 5–17 R_S, and thus can be compared to Figure 11 (left) with Cassini measurements at similar distances. The electron densities are typically somewhat greater than 10^5 cm^{-3} for noon local times for Voyager and Cassini measurements, and the dayside densities are in good agreement. However, the electron density at midnight was about an order of magnitude lower for the Voyager profile, i.e., there the electron density reached down to nearly 10^3 cm^{-3} whereas for the Cassini profiles the density on the nightside is typically around 10^4 cm^{-3} and rather goes down a bit below that in the early morning. The Voyager measurements might be somewhat problematic because for such low densities as 10^3 cm^{-3} the low-frequency cutoff is in a range from about 300–600 kHz where usually Saturn kilometric radiation (SKR) is the dominating emission. The observations numbered 7, 8, 9, 10, 13, and 14 of *Kaiser et al.* [1984] have cutoff frequencies below 600 kHz despite the fact that the SKR upper boundary is around 700 kHz for most of these observations. There are just a few cases with Cassini when the SEDs go down to the upper boundary of SKR, and in these cases the cutoff represents an upper limit. However, in the vast majority of cases the SED frequency cutoff is clearly above the SKR region even when the storm is on Saturn's nightside. Hence, the large numbers of Cassini profiles can be considered as more reliable as the single Voyager profile.

[32] Another comparison can be made to radio occultation data which reveals an electron density profile as function of altitude, but which can only be gained at local times around dawn and dusk since radio waves emitted by Cassini have to be picked up by terrestrial radio telescopes. However, it is possible to take a look at the peak electron density in those profiles. New radio occultation data by Cassini have revealed a systematic dependence of electron density with latitude; that is, it was found by *Kliore et al.* [2009] that peak electron densities increase with latitude. Seven radio occultations were done at midlatitudes from 27.7° to 43.6° planetodetic latitude (23.1° to 37.8° planetocentric), two of them at dawn and five of them at dusk. We plotted these measurements of *Kliore et al.* [2009, Table 1] as a function of solar zenith angle into our Figure 10 as blue triangles with 4 of them pointed upward for northern hemisphere measurements and 3 of them pointed downward for the southern hemisphere. It can be seen that the two dawn measurements match up pretty well with the SED results, whereas the dusk side radio occultations are more on the lower edge of the SED measurements, especially one of them (from orbit 72) which only gives a peak density around 5.4×10^3 cm^{-3}. However, four out of five radio occultation measurements at dusk were done at northern midlatitudes which points to a hemispherical asymmetry. The single radio occultation measurement from the southern hemisphere is in better agreement with the SED measurements that were done only with storms in the southern hemisphere.

[33] There are two more interesting features in Figure 10: The first one is the shift of points to higher densities around SZA = 140° (Figure 10, left). The absence of points at lower densities is probably due to the upper boundary of SKR which sometimes prevented a proper determination of the lower cutoff. The second feature is the asymmetry between left and right image indicating a fast rise of electron density in the morning side and a more gentle decrease due to recombination on the evening side.

4.3. Correlation to Solar EUV Fluxes

[34] How does the solar EUV flux, which via photoionization is usually the main source of ionization in planetary ionospheres [*Schunk and Nagy*, 2000], relate to Saturn ionospheric electron densities? To answer this question we plotted the solar EUV flux measured by the Solar Extreme Ultraviolet Monitor (SEM) on board the Solar and Heliospheric Observatory (SOHO) in Figure 12 as a function of time from the beginning of 2004 until the end of 2009. This EUV flux is normalized to a distance of 1 AU, it is measured in the wavelength range of 0.1 to 50 nm, and the flux data was downloaded from the Web page of the Space Sciences Center of the University of Southern California (http://www.usc.edu/dept/space_science/OLD_WEB/semdata.htm). Using the same abscissa we also plotted the maximum-to-minimum electron density ratios (diurnal variation) as given in section 4.1. The 6 values for the 6 SED storms lie in the range from about 10 to 60, which is indicated by the ordinate on the right-hand side of Figure 12. One can see a decreasing maximum-to-minimum ratio with decreasing solar EUV flux. The dashed lines are the error bars that are calculated as the sum of the relative variations of the maximum and minimum densities displayed in Figure 8 (A 50% relative error was taken for the minimum in three cases where the minimum consisted of only one measurement value). However, despite the large error bars, it is still highly probable that the diurnal variation goes down with decreasing

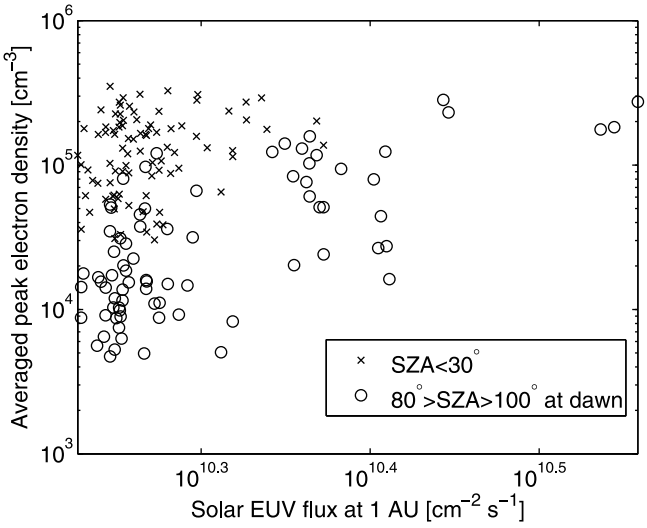

Figure 13. Averaged peak electron densities of Saturn's ionosphere plotted versus the daily averaged solar EUV flux as measured by SEM/SOHO. The circles indicate daily averages of peak electron densities with solar zenith angles (SZA) between 80° and 100° on the morning side. For the crosses the daily average in density is done for all values of solar zenith angles smaller than 30°, which are the local times of about ±2 h around noon. Most measurement values were gained after mid-2007 when the solar EUV flux was less than $10^{10.3} \approx 2 \times 10^{10}$ cm^{-2} s^{-1} as can be seen in Figure 12.

solar EUV flux, and this tendency is in fact in contradiction to theoretical models: *Moore et al.* [2004] predict a higher diurnal variation for solar minimum conditions since the ratio between the two main ions H^+/H_3^+ is smaller leading to more influence of the H_3^+ ion which exhibits a diurnal variation in density of 1–2 orders of magnitude. For solar maximum conditions the situation is the other way round, and a large ratio of H^+/H_3^+ means that the H^+ ion is dominant which should have little diurnal variation due to its long chemical lifetime.

[35] Not only the diurnal variation, but also the electron densities themselves show a decreasing tendency with decreasing solar EUV flux. This is shown in Figure 13 where one can see increasing electron densities with an increasing EUV flux. Two populations were plotted here: The circles are the electron densities averaged over the solar zenith angle interval 80° < SZA < 100° on the dawn side within 1 day, and they show a clear linear increase in the double-logarithmic plot versus the solar EUV flux. The highest-electron densities in the upper right corner of Figure 13 were measured in 2004 when the solar EUV flux was the highest, and all the values with solar fluxes higher than $10^{10.4}$ cm^{-2} s^{-1} were measured during storms ABC and E. Hence, the spacecraft distance might play some role here. The effect is less prominent for the crosses, which display the daily electron density averages for SZA < 30°. These solar zenith angles approximately correspond to ±2 h around local noon, and these local times were not sampled during 2004 or 2006. However, one can see no averaged electron densities smaller 10^5 cm^{-3} at high EUV fluxes. At least this tendency is consistent with the model of *Moore et al.* [2004], where higher-electron densities are obtained for solar maximum conditions.

4.4. Implications for Saturn's Ionosphere

[36] As mentioned in the introduction, past and current models of Saturn's ionosphere still cannot reproduce the diurnal variation as revealed by the SED measurements. However, theory and observations have become closer, because the new Cassini measurements indicate a diurnal variation of 1 to 2 orders of magnitude, which is almost 1 order of magnitude less compared to the Voyager result. In the model of *Moore et al.* [2004] the density of the H_3^+ ion exhibits a diurnal variation of 1 to 2 orders of magnitude, but this variation is mostly hidden below the higher density of the H^+ ion. Another open question is still the altitude of the peak electron density, and unfortunately SED measurements are not able to answer this question. The midlatitude radio occultations of *Kliore et al.* [2009] show peak altitudes of about 2600 to 2900 km for the dawn side. For dusk three radio occultations gave peak altitudes of 800 to 1200 km, and for two occultations the peaks were from 1500 to 1700 km. Peaks in Saturn's lower ionosphere below 800 km, which is a region not accessible to radio occultation measurements, could be due to meteoritic ions. The model of *Connerney and Waite* [1984] and constraints on the electron density due to the low attenuation of SEDs calculated by *Zarka* [1985b] actually suggest a strong decrease in electron density below the photochemical peak altitude.

[37] Our averaged profiles of Figures 8 or 9 give the electron density as a function of local time and therefore also allow an estimation of the change of electron density with local time or with time. Due to Saturn's fast atmospheric rotation of about 10.66 h at a latitude of 35°S 1 h of local time is traversed in only 0.444 h. A typical increase in electron density N_e at dawn can be described by an increase in 1 order of magnitude (from 10^4 cm^{-3} to 10^5 cm^{-3}) within 3 h of local time corresponding to 1.33 h in time. This can be approximated by the equation $N_e = 10^4 \times 10^{\frac{1}{1.33}t}$ with N_e in electrons per cm^3 and t in hours. Such an increase can be seen for SED storms F^1 and F^2 from about 5–8 LT or 6–9 LT. The semilogarithmic plots of Figure 8 show a linear increase in the logarithm of the electron density. Calculating the time derivative of the previous equation one arrives at $\frac{dNe}{dt} = \frac{\ln 10}{1.33} \times 10^4 \times 10^{\frac{1}{1.33}t}$. Inserting the time interval from $t = 0$ to $t = 1.33$ h we retrieve temporal changes in electron density from 1.73×10^4 to 1.73×10^5 cm^{-3} h^{-1}. This can be identified as electron production rates ranging from about 5 to 50 cm^{-3} s^{-1} from local times in the early morning to late morning. The negative slope giving the loss rate at dusk is somewhat more gentle indicating a slower recombination process. Our rates are somewhat higher than predicted by the model of *Moore et al.* [2004], who estimate the peak production to be around 10 cm^{-3} s^{-1} for H_3^+ and 0.6 cm^{-3} s^{-1} for H^+ for solar maximum and overhead illumination. These *Moore et al.* [2004] peak production rates do not represent the rate of change in electron density, as derived above for the SED observations, because there is still ion loss to be accounted for. Therefore, at least in Saturn's photochemical regime, there is a sizable disconnect

between the model-predicted ion production rates and the SED-derived ion production rates.

[38] Additional photochemistry must be considered in order to induce any diurnal variation in peak electron densities since the H^+ loss due to radiative recombination yields an H^+ lifetime of more than 1 Saturn day. The models in the past have typically introduced some combination of neutral water influx and/or vibrationally excited H_2 chemistry in order to convert the long-lived H^+ ions into short-lived molecular ions. These processes reduce the modeled electron density and increase the altitude of the peak electron density [*Majeed and McConnell*, 1996; *Moses and Bass*, 2000; *Moore et al.*, 2004] to better match the observations. These additional loss processes, however, are not particularly well-constrained. Moreover, if they are allowed to act at all Saturn local times, then they further exacerbate the disconnect between the SED-derived ion production rates and the model-estimated production rates during the morning buildup of electron densities from 10^4 cm^{-3} to 10^5 cm^{-3}.

[39] The observing geometry with Cassini in the northern hemisphere observing the southern storm led to a few hundred SED episodes where the radio waves actually had to penetrate Saturn's rings to be observed by the RPWS instrument. Since some ring particles can have a size of a few meters, there could be an influence for SEDs at higher frequencies where the wavelength is of the order of the ring particle size [*Burns et al.*, 1983]. We found a few cases where gaps in SED activity or bite-outs at lower frequencies were observed. However, bite-outs or gaps also happened when SEDs didn't have to go through the rings. In the vast majority of cases (~95%) the SEDs seem to propagate through the rings without any obvious effect. There might be effects at higher frequencies, but RPWS measurements can only go up to 16 MHz. Since the wavelength is 300 m at 1 MHz, we don't expect and did not find an influence of Saturn's rings on the low-frequency cutoff. The ion and electron densities close to the rings (~1 cm^{-3} [*Waite et al.*, 2005]) as well as in Saturn's plasma disk (<100 cm^{-3} [*Persoon et al.*, 2006]) are too small to have any effect on the propagation of high-frequency SED radio waves.

5. Conclusions and Outlook

[40] Certainly, radio wave propagation in Saturn's ionosphere is worth further studies by ray tracing since there are significant radio wave propagation effects when Cassini observes the SED storm rising and setting. We call this the 'over-horizon effect' and a first preliminary modeling was done by *Zarka et al.* [2006]. In our study here we restrict our peak electron density measurements of Saturn's ionosphere to angles of incidence $\alpha < 60°$ to avoid such propagation effects and assume straight line propagation. Until the end of 2009 there were 231 SED episodes with enough SEDs to draw the so-called low-frequency cutoff (f_{cutoff}), a line below which no SEDs are observed propagating to the spacecraft. Combined observations of Cassini/ISS and ground-based telescopes allowed a determination of the locations of the SED storms, which were all located at a planetocentric latitude of 35°S. This knowledge of the geometrical situation is essential to determine the peak plasma frequency $f_{pe,peak}$ of Saturn's ionosphere via the relation $f_{pe,peak} = f_{cutoff} \cos(\alpha)$ as a function of the local time of the storm. We averaged the profiles and found a diurnal variation in electron density between one and 2 orders of magnitude, which is somewhat less compared to the Voyager result which indicated more than 2 orders of magnitude between day and nightside. The diurnal variation as well as the electron density also decrease from 2004 until 2009 which probably correlates to the decrease in EUV flux during this relatively quiet period of the sun. The peak electron densities at noon are usually somewhat greater than 10^5 cm^{-3}, at midnight they are typically around 10^4 cm^{-3}, and at dawn and dusk around 5×10^4 cm^{-3} with a large variability which roughly agrees with radio occultation data obtained at mid-latitudes. There is some systematic influence of the measured electron densities with spacecraft distance. Profiles gained at close distances (within 14 R_S) sometimes show electron densities with a factor of 2 smaller compared to larger distances. Close distance profiles also show a clear minimum in electron density in the early morning from about 04–05 LT. Since Cassini continues its mission until 2017 we can expect more measurements in future that could confirm the relation of Saturn's ionospheric electron density to the EUV flux of the sun and also allow measurements at different latitudes in case future SED storms appear in equatorial regions or 35°N.

[41] **Acknowledgments.** G. F. was supported by a grant (project P21295-N16) from the Austrian Science Fund (FWF) and by a short-term research scholarship at the University of Iowa funded by NASA through contract 1356500 from the Jet Propulsion Laboratory. The International Space Science Institute (ISSI) in Bern, Switzerland, is acknowledged for hosting two meetings of the ISSI International Team on Saturn Aeronomy (number 166). The team of the CELIAS/SEM experiment on board the SOHO spacecraft is acknowledged for providing the solar EUV fluxes via its Web page at the Space Sciences Center of the University of Southern California. G. F. thanks his trainee Dino Mehic for his help with data processing. Many amateurs observed Saturn with their optical telescopes and helped in the determination of the storm locations. Among them, G. F. specially thanks T. Barry, M. Delcroix, C. Go, D. Peach, R. Vandebergh, and A. Wesley.

[42] Masaki Fujimoto thanks the reviewers for their assistance in evaluating this paper.

References

Burns, J. A., M. R. Showalter, J. N. Cuzzi, and R. H. Durisen (1983), Saturn's electrostatic discharges: Could lightning be the cause?, *Icarus*, *54*, 280–295.

Cecconi, B., and P. Zarka (2005), Direction finding and antenna calibration through analytical inversion of radio measurements performed using a system of two or three electric dipole antennas on a three-axis stabilized spacecraft, *Radio Sci.*, *40*, RS3003, doi:10.1029/2004RS003070.

Connerney, J. E. P., and J. H. Waite (1984), New model of Saturn's ionosphere with an influx of water from the rings, *Nature*, *312*, 136–138.

Davies, K. (1990), *Ionospheric Radio*, Peter Peregrinus, London.

Delcroix, M., and G. Fischer (2010), Contribution of amateur observations to Saturn storm studies, paper presented at European Planetary Science Congress 2010, Rome.

Dyudina, U. A., A. P. Ingersoll, P. E. Shawn, C. C. Porco, G. Fischer, W. S. Kurth, M. D. Desch, A. Del Genio, J. Barbara, and J. Ferrier (2007), Lightning storms on Saturn observed by Cassini ISS and RPWS in the years 2004–2006, *Icarus*, *190*, 545–555.

Dyudina, U. A., A. P. Ingersoll, S. P. Ewald, C. C. Porco, G. Fischer, W. S. Kurth, and R. A. West (2010), Detection of visible lightning on Saturn, *Geophys. Res. Lett.*, *37*, L09205, doi:10.1029/2010GL043188.

Evans, D. R., J. H. Romig, C. W. Hord, K. E. Simmons, J. W. Warwick, and A. L. Lane (1982), The source of Saturn electrostatic discharges, *Nature*, *299*, 236–237.

Fischer, G., et al. (2006), Saturn lightning recorded by Cassini/RPWS in 2004, *Icarus*, *183*, 135–152.

Fischer, G., W. S. Kurth, U. A. Dyudina, M. L. Kaiser, P. Zarka, A. Lecacheux, A. P. Ingersoll, and D. A. Gurnett (2007), Analysis of a giant lightning storm on Saturn, *Icarus*, *190*, 528–544.

Gurnett, D. A., et al. (2004), The Cassini radio and plasma wave science investigation, *Space Sci. Rev.*, *114*, 395–463.

Hunt, G. E., D. Godfrey, J. -P. Müller, and R. F. T. Barrey (1982), Dynamical features in the northern hemisphere of Saturn from Voyager 1 images, *Nature*, *297*, 132–134.

Kaiser, M. L., J. E. P. Connerney, and M. D. Desch (1983), Atmospheric storm explanation of Saturnian electrostatic discharges, *Nature*, *303*, 50–53.

Kaiser, M. L., M. D. Desch, and J. E. P. Connerney (1984), Saturn's ionosphere: Inferred electron densities, *J. Geophys. Res.*, *89*(A4), 2371–2376.

Kliore, A. J., A. F. Nagy, E. A. Marouf, A. Anabtawi, E. Barbinis, D. U. Fleischman, and D. S. Kahan (2009), Midlatitude and high-latitude electron density profiles in the ionosphere of Saturn obtained by Cassini radio occultation observations, *J. Geophys. Res.*, *114*, A04315, doi:10.1029/2008JA013900.

Lindal, G. F., D. N. Sweetnam, and V. R. Eshleman (1985), The atmosphere of Saturn: An analysis of the Voyager radio occultation measurements, *Astron. J.*, *90*, 1136–1146.

Majeed, T., and J. C. McConnell (1996), Voyager electron density measurements on Saturn: Analysis with a time dependent ionospheric model, *J. Geophys. Res.*, *101*(E3), 7589–7598.

Martyn, D. F. (1935), The propagation of medium radio waves in the ionosphere, *Proc. Phys. Soc.*, *47*(2), 323–339.

Mendillo, M., L. Moore, J. Clarke, I. Müller-Wodarg, W. S. Kurth, and M. L. Kaiser (2005), Effects of ring shadowing on the detection of electrostatic discharges at Saturn, *Geophys. Res. Lett.*, *32*, L05107, doi:10.1029/2004GL021934.

Moore, L., M. Mendillo, I. Müller-Wodarg, and D. L. Murr (2004), Modeling of global variations and ring shadowing in Saturn's ionosphere, *Icarus*, *172*, 503–520.

Moore, L., A. F. Nagy, A. J. Kliore, I. Müller-Wodarg, J. D. Richardson, and M. Mendillo (2006), Cassini radio occultations of Saturn's ionosphere: Model comparisons using a constant water flux, *Geophys. Res. Lett.*, *33*, L22202, doi:10.1029/2006GL027375.

Moses, J. I., and S. F. Bass (2000), The effects of external material on the chemistry and structure of Saturn's ionosphere, *J. Geophys. Res.*, *105*(E3), 7013–7052.

Nagy, A. F., et al. (2006), First results from the ionospheric radio occultations of Saturn by the Cassini spacecraft, *J. Geophys. Res.*, *111*, A06310, doi:10.1029/2005JA011519.

Nagy, A. F., A. J. Kliore, M. Mendillo, S. Miller, L. Moore, J. I. Moses, I. Müller-Wodarg, and D. Shemansky (2009), Upper atmosphere and ionosphere of Saturn, in *Saturn From Cassini-Huygens*, edited by M. K. Dougherty, L. W. Esposito, and S. M. Krimigis, pp. 181–202, Springer, Dordrecht, Neth.

Persoon, A. M., D. A. Gurnett, W. S. Kurth, and J. B. Groene (2006), A simple scale height model of the electron density in Saturn's plasma disk, *Geophys. Res. Lett.*, *33*, L18106, doi:10.1029/2006GL027090.

Porco, C. C., et al. (2005), Cassini imaging science: Initial results on Saturn's atmosphere, *Science*, *307*, 1243–1247.

Rakov, V. A., and M. A. Uman (2003), *Lightning: Physics and Effects*, Cambridge Univ. Press, Cambridge, U. K.

Schunk, R. W., and A. F. Nagy (2000), *Ionospheres*, Cambridge Univ. Press, New York.

Sromovsky, L. A., H. E. Revercomb, R. J. Krauss, and V. E. Suomi (1983), Voyager 2 observations of Saturn's northern midlatitude cloud features: Morphology, motions, and evolution, *J. Geophys. Res.*, *88*(A11), 8650–8666.

Waite, J. H., et al. (2005), Oxygen ions observed near Saturn's A ring, *Science*, *307*, 1260–1262.

Warwick, J. W., et al. (1981), Planetary radio astronomy observations from Voyager 1 near Saturn, *Science*, *212*, 239–243.

Zarka, P. (1985a), Directivity of Saturn electrostatic discharges and ionospheric implications, *Icarus*, *61*, 508–520.

Zarka, P. (1985b), On detection of radio bursts associated with Jovian and Saturnian lightning, *Astron. Astrophys.*, *146*, L15–L18.

Zarka, P., and B. M. Pedersen (1983), Statistical study of Saturn electrostatic discharges, *J. Geophys. Res.*, *88*(A11), 9007–9018.

Zarka, P., B. Cecconi, L. Denis, W. M. Farrell, G. Fischer, G. B. Hospodarsky, M. L. Kaiser, and W. S. Kurth (2006), Physical properties and detection of Saturn's radio lightning, in *Planetary Radio Emissions VI*, edited by H. O. Rucker, W. S. Kurth, and G. Mann, pp. 111–122, Austrian Acad. Sci. Press, Vienna.

U. A. Dyudina, Geological and Planetary Sciences, California Institute of Technology, MC 150-21, Pasadena, CA 91125, USA.

G. Fischer, Space Research Institute, Austrian Academy of Sciences, Schmiedlstr. 6, A-8042 Graz, Austria. (georg.fischer@oeaw.ac.at)

D. A. Gurnett, Department of Physics and Astronomy, University of Iowa, 203 Van Allen Hall, Iowa City, IA 52242, USA.

L. Moore, Center for Space Physics, Boston University, 725 Commonwealth Ave., Boston, MA 02215, USA.

P. Zarka, Observatoire de Paris, 5 Pl. Jules Janssen, F-92195 Meudon CEDEX, France.